

**SAE TECHNICAL  
PAPER SERIES**

**2007-01-1589**

---

# Comprehensive Modeling of Automotive Ignition Systems

**R. C. Stevenson and R. Palma**  
Visteon/ACH-LLC, CAE

**C. S. Yang, S. K. Park and C. Mi**  
University of Michigan, Dearborn

Reprinted From: **Automotive Electronics and Systems Reliability  
(SP-2088)**

ISBN 0-7680-1633-9



9 780768 016338

**SAE** *International*<sup>™</sup>

2007 World Congress  
Detroit, Michigan  
April 16-19, 2007

By mandate of the Engineering Meetings Board, this paper has been approved for SAE publication upon completion of a peer review process by a minimum of three (3) industry experts under the supervision of the session organizer.

All rights reserved. No part of this publication may be reproduced, stored in a retrieval system, or transmitted, in any form or by any means, electronic, mechanical, photocopying, recording, or otherwise, without the prior written permission of SAE.

For permission and licensing requests contact:

SAE Permissions  
400 Commonwealth Drive  
Warrendale, PA 15096-0001-USA  
Email: [permissions@sae.org](mailto:permissions@sae.org)  
Fax: 724-776-3036  
Tel: 724-772-4028



For multiple print copies contact:

SAE Customer Service  
Tel: 877-606-7323 (inside USA and Canada)  
Tel: 724-776-4970 (outside USA)  
Fax: 724-776-0790  
Email: [CustomerService@sae.org](mailto:CustomerService@sae.org)

**ISSN 0148-7191**

**Copyright © 2007 SAE International**

Positions and opinions advanced in this paper are those of the author(s) and not necessarily those of SAE. The author is solely responsible for the content of the paper. A process is available by which discussions will be printed with the paper if it is published in SAE Transactions.

Persons wishing to submit papers to be considered for presentation or publication by SAE should send the manuscript or a 300 word abstract of a proposed manuscript to: Secretary, Engineering Meetings Board, SAE.

**Printed in USA**

# Comprehensive Modeling of Automotive Ignition Systems

**R. C. Stevenson and R. Palma**  
Visteon/ACH-LLC, CAE

**C. S. Yang, S. K. Park and C. Mi**  
University of Michigan, Dearborn

Copyright © 2007 SAE International

## ABSTRACT

This paper presents a comprehensive approach to improve the analysis and design process of automotive ignition coils. The delivered voltage and energy of the coil to the spark plug load are the two essential requirements placed on a coil design. The prediction of these two quantities, derived from the simulated transient secondary current and voltage, is fundamental to the design process and allows early assessment of design robustness. With only the data required for electromagnetic finite element analysis (FEA), including material loss data, the magnetic and electrostatic interactions among the coil laminations and windings can be modeled. These field computations are converted to equivalent circuit elements employed in a systems model. The systems model allows the calculation of requisite transient signals. This approach is highly flexible and gives fast simulations. Good agreement was obtained between the test data and the simulation results in both the time-domain and the frequency-domain.

## INTRODUCTION

The objective of this work is to provide tools and methods to improve the design process, and ultimately to improve the design and performance of automotive ignition coil systems. These modeling efforts allow the early assessment of design robustness and improve the reliability of the automotive ignition coil system. The analysis of the ignition coil system discussed here includes a driver, a coil, and a load. Ignition coils deliver the high voltage (several tens of kV) necessary to initiate the breakdown of the sparkplug gap, and then sufficient energy (several tens of mJ) to sustain the combustion, and overcome plug losses. The delivered kV and energy are the two essential requirements imposed on the ignition coil design. These two quantities, as well as other parameters, are derived from simulated transient signals of the coil, i.e., the primary and secondary currents and voltages. The accurate prediction of the time variation of these quantities is fundamental to the design process. The proposed approach is from first principles to the extent possible. The number of

experimentally determined factors from actual coil prototypes was minimized in predicting the coil behavior. A coil design process was developed that begins with only dimensions, material properties, and topology. Then the non-linear magnetic and linear electrostatic interactions among the windings and laminations of the coil were modeled using electromagnetic finite element analysis (FEA). A simple model was developed to account for the winding resistance. The proposed approach is to convert field computations into equivalent circuit elements to be employed in a systems modeling program. The equivalent circuit approach allows a high degree of flexibility, and relatively fast time-transient simulations. The physical modeling is with static magnetic and electric fields, but the system simulator properly accounts for dynamic effects through an interpolation process. In addition to the coil model, the equivalent circuit models for the electronic driver and sparkplug load must be included. However, the parameters and physics of these two subsystems are less well known, or harder to obtain, than for the coil itself.

The rest of the paper is arranged as follows: First, the motivation, objectives, and the approach of the proposed work are discussed. Next, the basic coil behavior is demonstrated in terms of a Fundamental Coil Model. Then more complex behavior is introduced in terms of Simple Coil Model. Simulations are given for the Simple Coil Model that illustrates the effects on signals from non-linear components. Following this Simple Coil Model, the detailed modeling of the individual components of the Comprehensive Systems Model is presented. Finally, the simulated results are compared with measured data, on a particular developmental coil, in the time domain and frequency domain.

## IGNITION COIL MODELING

### MOTIVATION, OBJECTIVES AND APPROACH

#### Motivation:

The motivation to pursue a comprehensive modeling effort for ignition coils is several-fold, and common to

most engineering modeling efforts. A good model promotes basic physical understanding of the surprisingly complex operation of ignition coils. It allows the design engineer to pose “what if” questions, which can generally be answered relatively quickly. Most importantly, it reduces cost in terms of the number of prototypes, the testing, and the time dedicated to building physical prototypes.

There is scant to non-existent literature on the modeling of automotive ignition coils [1]. There appears to be little or no literature on electromagnetic FEA modeling of ignition coils. Design methods for coils seem to be closely held secrets in the industry, and most design work appears to be done from historical precedence.

Design modifications in the past have been guided by basic transformer theory, without resorting to detailed modeling. The construction of coil prototypes, typically with several design iterations, is an expensive and a time consuming process. It involves the specification and fabrication of annealed laminations, the design and fabrication of bobbins and packaging, the winding of the primary and secondary coils, the potting the coils, and the testing the coils. This type of prototyping can have cycle times of several months. By comparison, modeling can produce comparable answers with in a week or less.

### Objectives

Given these prototyping costs, both temporal and financial, the objectives of this modeling work become apparent: reduce cost by minimizing the need to build prototypes. To this end, the electromagnetic engineer should create a modeling process whose short-term objective provides accurate guidance for the design engineer during initial screening of design variations. As a derivative of this goal, the prototypes that are built with the modeling guidance should be close to the design objectives. These goals require that the modeling effort should be based on “first principles” to the extent possible. It is to predict accurate transient behavior, not to fit the model to data gathered after prototypes are built, that the modeling effort is directed. However, because of the magnetic, electrical, and geometrical complexity of the coils, modeling approximations are inherent. Thus, some adjustment of systems and models to test data may be necessary.

The longer-term objective is to advance from an analysis of design to a synthesis of design. That is, given a set of specifications, produce an optimized design that accounts for constraints on performance, material costs, package space, etc. This type of design work requires having an analysis procedure coupled to the ability to iterate, sample, or search many designs subject to the constraints. There is likely no unique solution. This longer-term objective will be accomplished in future work.

### Approach

With regard to the modeling approaches, there are at least three potentially viable schemes. The first scheme, and the most physically accurate, would be to solve the complete set of Maxwell equations, beyond the low-frequency approximation which is generally used for electric machine modeling. In this complete formulation, Ampere’s Law ( $\nabla \times \mathbf{H} = \partial_t \mathbf{D} + \mathbf{J}$ ) includes the displacement current density,  $\partial_t \mathbf{D}$ , while in the low-frequency case, the displacement current density is ignored. For this scheme, the full coupling of the electric and magnetic fields is obtained, i.e., the magnetic inductive and capacitive effects are automatically accounted. For the current state of the art in electromagnetic solvers, the direct solution of the complete set of Maxwell equations, with strong material nonlinearity, is not practical.

A second approach is to solve a transient FEA model of the magnetics, including external circuitry for the driver, the load, and capacitive effects. This approach is feasible but cumbersome, since a transient magnetic FEA problem would need to be solved for changes in any minor model parameter.

A third approach, detailed in this paper, is a more flexible method. In this third approach, the model includes an equivalent circuit of the driver, the load, and the coil. The lumped circuit elements for inductive, capacitive, and resistive effects are obtained from FEA. The inductive elements account for non-linear material properties. The flexibility of this approach comes with studies requiring changes to circuit elements, other than those derived from FEA. These changes can be accommodated quickly and easily. Simulations can be run in a matter of a few minutes.

### IGNITION COIL OPERATION OVERVIEW

Automotive ignition system requirements and operation with regard to engine and spark plug performance is discussed in [2]. For the modeling effort described in this section, the focus is more narrowly on describing how the coil works. The ignition coil system consists of a coil, which acts as a transient voltage transformer; a driver, which “charges” the primary winding; and a load (a spark plug) to which the coil delivers a high voltage pulse. The coil system block diagram is shown Fig. 1. The basic job of an ignition coil system is to convert a low-voltage DC source into a very high voltage and very fast transient at the spark plug gap.

### Driver

The driver part of the system consists of a voltage source (the automotive battery, nominally 14.4 V) and a controlled switch. The switching device is commonly an IGBT [3]. However, this simple switch will not suffice, because the large voltage that develops in the

secondary is transformed by the coil to the so-called “fly-back voltage” in the primary. The fly-back voltage may be over 1,000V. IGBTs used for ignition can withstand no more than approximately 600 V across the Emitter-Collector ports. Thus, the IGBT must be protected against the fly-back voltages. This protection comes in the form of a clamping Zener diode added across the IGBT. This diode has an avalanche voltage of about 500 V. This diode has a major effect on the signal dynamics.

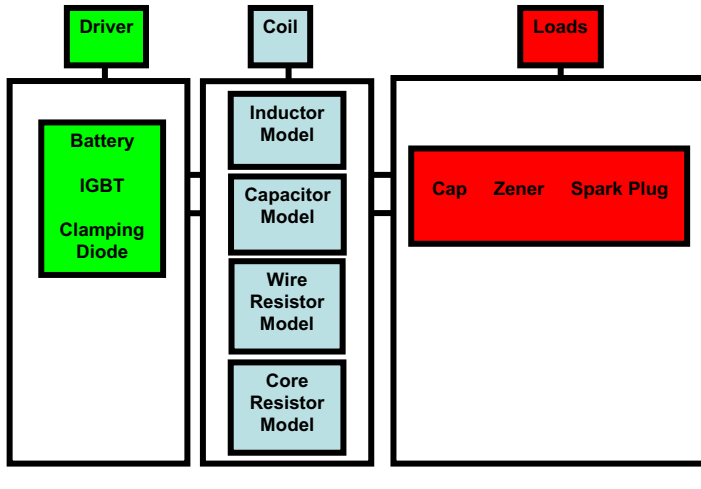


Fig. 1. Component for ignition coil system.

Coil

The ignition coil is a (transient) voltage transformer. A schematic representation of the ignition coil is shown Fig. 2. The primary and secondary windings are coupled through a magnetic circuit of laminated steel, which channels magnetic flux much like a wire conducts current. However, the magnetic “conductivity,” i.e., the permeability of the laminations, is much lower than the corresponding electrical conductivity of wire. Thus, magnetic fields leak more from a magnetic circuit than the electric fields leak from an electrical wire. Fig. 2 represents this leakage as a primary and a secondary leakage flux. Leakage flux represents a loss of coupling between the primary and the secondary windings. Not all the flux generated by the primary winding links the secondary winding, and vice versa. Leakage flux may appear to be innocuous, since the non-ideal coupling for an ignition coil can approach 99%. However, it can be seen that the leakage flux results in a mode that appears in transient operation, but is not apparent in steady state operation.

Arguably, the most significant parameter of a transformer is the turns ratio,  $\epsilon = N_s / N_p$ , where  $N_p$  and  $N_s$  are the number of turns of the primary and the secondary winding, respectively. Given a primary winding, typically with  $N_p \sim 100$  turns, and a secondary

winding, typically with  $N_s \lesssim 10,000$  turns, the turns ratio is about  $\epsilon \lesssim 100$ . Power conservation implies that the primary voltage and the secondary voltage are related by  $v_s = \epsilon v_p$ , while the primary current and secondary current are related by,  $i_s = i_p / \epsilon$ . For example, if the avalanche voltage of the clamping Zener Diode is about 500 volts, with  $\epsilon = 100$ , the peak secondary voltage is no more than 50 kV. Correspondingly, if the peak primary current is 10 A, then the peak secondary current is 100 mA.

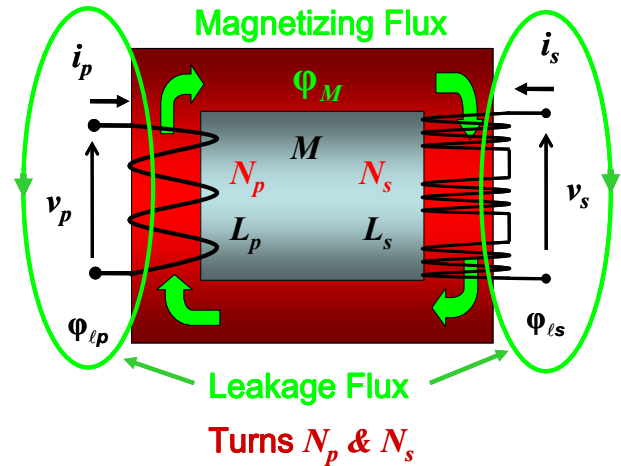


Fig. 2. Transformer magnetic circuit model

In practice, the so-called “negative” voltage  $v_n$  is measured instead of  $v_p$ . Since for peak values,  $v_n \gg V_b$ , then

$$v_p = V_b - v_n \approx -v_n.$$

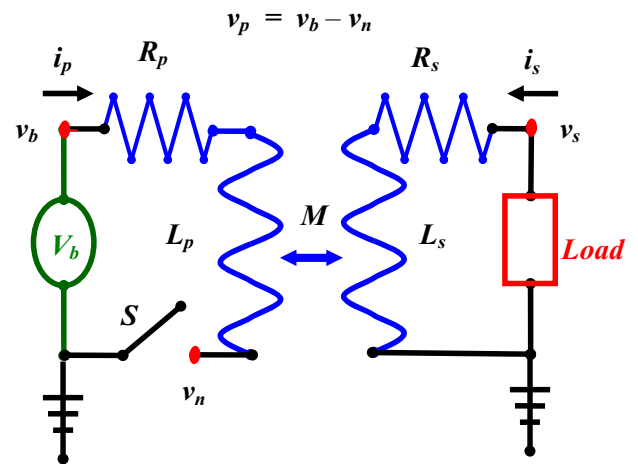


Fig. 3. Fundamental Circuit Model for coil.

To examine the operation of the coil from a transient point of view, consider the simplified equivalent circuit

representation of the coil system, as shown in Fig. 3. To create the large secondary voltage transient, there are several steps. First, the driver closes the switch  $S$ , a battery with voltage  $V_b$ , “charges” the primary coil up to a peak current  $I_{max}$  of about 10 A. The charging rate depends on the primary time constant,  $\tau_p = L_p / R_p$ . As soon as  $I_{max}$  is reached, the driver opens the switch,  $S$ . The current in the primary winding is cut off; the flux generated by the primary winding,  $\phi_p$ , collapses in a time interval,  $\Delta\tau \sim 10 \mu s$ . The primary flux is composed of two parts, the primary leakage flux,  $\phi_{lp}$  and the magnetizing flux,  $\phi_M$ , which links the secondary coil through  $N_s$  turns. This time changing flux in the secondary coil creates a time changing secondary voltage through Faraday’s Law:

$$v_s = N_s \frac{d}{dt} \phi_M.$$

### Loads

The modeling in this paper does not focus primarily on the spark plug, as a load. The reason for not using a spark plug directly is that spark plugs are notoriously variable. A reproducible standard spark plug load would be hard to maintain. For the characterization of actual prototypes, there are two different loads, which correspond to two standard tests. The tests are the peak voltage test ( $kV$  test) and the energy test ( $E$  test), respectively.

For the  $kV$  test, a capacitor is employed which matches the estimated or measured capacitive load that the spark plug would experience while in situ in the engine block, prior to spark gap breakdown. Thus, the peak secondary voltage buildup just prior to breakdown can be measured.

For the  $E$  test, the spark plug, after gap breakdown, is simulated during the glow portion of the ignition event. Zener diodes are inserted in series, whose cumulative avalanche voltage is 800 V, which is the approximate constant voltage that appears across a spark gap during the glow phase. Time-integration of the power dissipated across the Zener will give a measure of the total energy output during the ignition event.

### IGNITION COIL OPERATION: SIMPLE COIL MODEL

#### Simple Coil Model

A number of scenarios are modeled in this section based on the Simple Circuit Model of Fig. 4. By adding additional components to the fundamental circuit of Fig. 3, more realistic simulation is produced. The idea is to use the insight gained from this simple model to interpret what is observed with actual transient data and

simulations of the more complex Comprehensive Systems Model. The circuit is solved with the aid of the *Simplorer* [4] modeling tool. The characteristic transient signals,  $i_p, v_p$  (or  $v_n$ ),  $i_s$ , and  $v_s$  are affected, as additional components are added. It is shown below how signals change for different loads in the  $kV$  test and in the  $E$  test, for imperfect transformer coupling, or a clamping diode across the switch, or a parasitic capacitance  $C_{ps}$ . For the  $kV$  Test the load is a capacitor, while for the  $E$  test, the load is modeled as a constant voltage source that turns on when the breakdown of the gap occurs.

The primary and secondary voltages and currents are plotted together on the same graph. In all plots, the primary voltage is scaled by the turns ratio of 100, and the secondary current by the same factor. This allows an easier comparison of the corresponding behavior. Table I lists the parameters of the study coil.

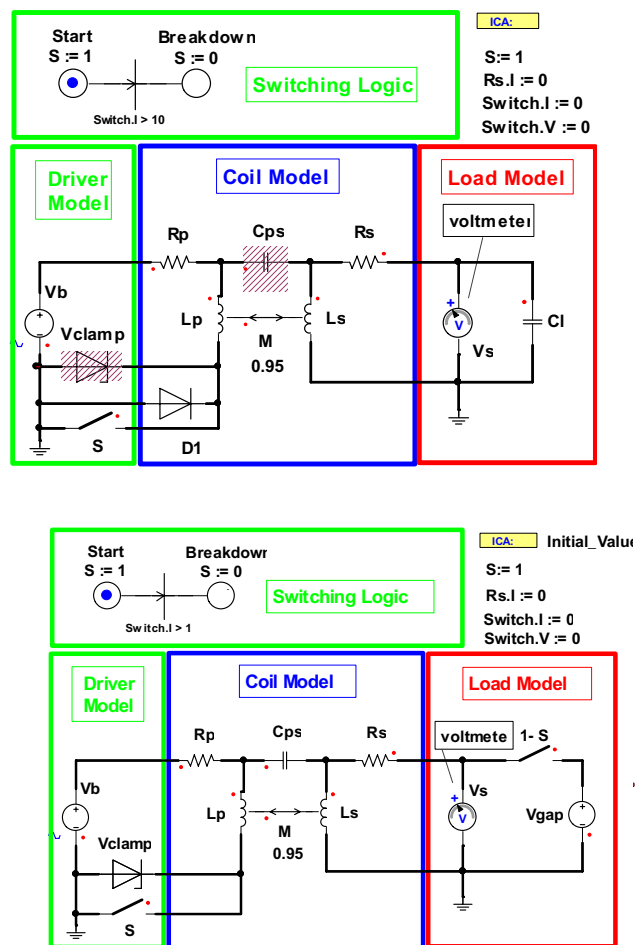


Fig. 4. The Simple Coil Model for an ignition coil system constructed in the simulation package *Simplorer*. The figure shows two different coil loads: A capacitor is for the  $kV$  test, and a switched voltage source is for the  $E$  test. The coupling constant may be changed. There are additional components in this circuit, compared with the fundamental coil circuit: There is a Zener clamping diode, and parasitic capacitor coupling the primary and secondary.

Case I. Simple Coil Model,  $kV$  test.

Case Ia.  $k = 1.0$ , no clamping diode, no  $C_{ps}$ .

This case is a baseline case: the fundamental coil with a capacitive load. The simulated results are shown in Fig. 5a. It can be seen from Fig. 5a that in the transient case, the voltage and current ratios follow closely the ideal transformer law. The secondary voltage does not resemble a fast transient spike typical for an ignition event, but is a decaying sinusoid.

Case Ib.  $k = 0.95$ , no clamping diode, no  $C_{ps}$ .

In this case, the imperfect coupling in the coil is introduced. The simulated results are shown in Fig. 5b. It can be seen from Fig. 5b, that the imperfect coupling leads to damped ringing in the signals. This ringing is at a higher frequency, roughly by a factor of two, above the ringing frequency in the secondary, in the case of perfect coupling. The imperfect coupling introduces an additional mode, and changes the character of existing modes. There is ringing in the startup portions of the primary and secondary currents, as well as the secondary voltage, where there was none for perfect coupling. In addition, there is a delta-function-like spike in the primary voltage, where one does not exist in the fundamental coil simulation. This spike is the so-called "leakage inductance pulse".

Table 1. Parameters for Simple coil

| Parameter              | Value     | Unit       |
|------------------------|-----------|------------|
| $V_b$                  | 14.2      | V          |
| $V_{clamp}$            | 500       | V          |
| $L_p$                  | 1         | mH         |
| $L_s$                  | 10        | H          |
| $k$                    | 1.0, 0.95 | no unit    |
| $M = k \sqrt{L_p L_s}$ | 100, 95   | mH         |
| $R_p$                  | 0.5       | $\Omega$   |
| $R_s$                  | 5000      | $\Omega$   |
| $R_{clamp}$            | 1         | m $\Omega$ |
| $R_{for}$              | 1         | m $\Omega$ |
| $R_{rev}$              | 100       | k $\Omega$ |
| $C_\ell$               | 10        | pF         |
| $C_{ps}$               | 10        | pF         |
| $V_{gap}$              | - 800     | V          |

Case Ic.  $k = 1.0$ , with clamping diode, no  $C_{ps}$ .

When a Zener clamping diode is added [5], there is a radical change in the characteristic signals. It can be seen from Fig. 5c that the clamping diode allows only one half-cycle in the primary voltage, and it clips the voltage at 500V level. However, there are also some residual effects on the primary current signal due to the diode's presence in the circuit, specifically the diode's  $I-V$  characteristics. The primary current shows, subsequent to the main charging curve, a positive going pulse, due to the avalanche portion of the diode's characteristics, followed by a negative going pulse, due to the forward characteristics. The  $I-V$  characteristics of a Zener diode might be represented by a piecewise linear model as in Fig. 6. The height of the first pulse depends on the resistance  $R_{clamp}$  of the avalanche portion of the Zener  $I-V$  characteristics. The width of the pulse depends on time that primary voltage exceeds the voltage  $V_{clamp}$ . With regard to the negative going pulse, its height depends on the resistance  $R_{for}$  of the forward characteristic curve of the Zener diode. The large reverse resistance  $R_{rev}$  prevents positive current flow in the primary; the negative going pulse bleeds away due to the resistance in the primary.

Case Id.  $k = 0.95$ , with clamping diode, no  $C_{ps}$ .

By turning on the imperfect coupling, it can be seen from Fig. 5d that a damped ringing is introduced back into the transient signals.

Case Ie.  $k = 0.95$ , with clamping diode, with  $C_{ps}$ .

A capacitor is added to the model, which accounts for electrostatic coupling between the primary and secondary windings. A drop in the secondary voltage is expected because the capacitor should draw energy away from the winding. In Fig. 5e, with a 10 pF coupling capacitor, there is a 10,000 V drop in the peak secondary voltage. The secondary voltage transient is also more rounded, probably resulting from capacitive filtering. In addition, there is a corresponding drop in the diode-induced current pulses mentioned in Case Ic above.

Case II. Simple Coil Model,  $E$  Test.

This section discusses the  $E$  Test load to examine how the characteristic coil signals change for the various experiments performed for the  $kV$  Test.

Case IIa.  $k = 1.0$ , no clamping diode, no  $C_{ps}$ .

Fig. 7a shows the simulation for this baseline case. The important signal is the secondary current. Upon the switching of the primary current at time  $t = \tau_B$ , the secondary current jumps to a finite value, and then decays in a characteristic triangular waveform. Observe

that the simulation is valid only to the time when the secondary crosses zero, at time,  $t = \tau_B + \tau_{SD}$ , even though the simulated signal goes beyond. At  $t = \tau_B + \tau_{SD}$ , the true ignition would stop. The length of the secondary current pulse is called the spark duration,  $\tau_{SD}$ . The energy delivered to the gap can be calculated:

$$E = \int_{\tau_B}^{\tau_B + \tau_{SD}} dt i_s(t) V_{gap}.$$

Case IIb.  $k = 0.95$ , no clamping diode, no  $C_{ps}$ .

As shown in Fig. 7b, it can be seen that the effect of resorting to imperfect coupling appears to be minimal.

The delta function spike does appear in the primary voltage waveform at the switching time  $\tau_B$ .

Case IIc.  $k = 0.95$ , with clamping diode, no  $C_{ps}$ .

From Fig. 7c., the clamping diode has minimal to no effect on the characteristic waveforms.

Case IIId.  $k = 0.95$ , with clamping diode, with  $C_{ps}$ .

With the addition of a coupling capacitor  $C_{ps}$ , it can be seen from Fig. 7d that there is an additional damped sinusoidal mode created.

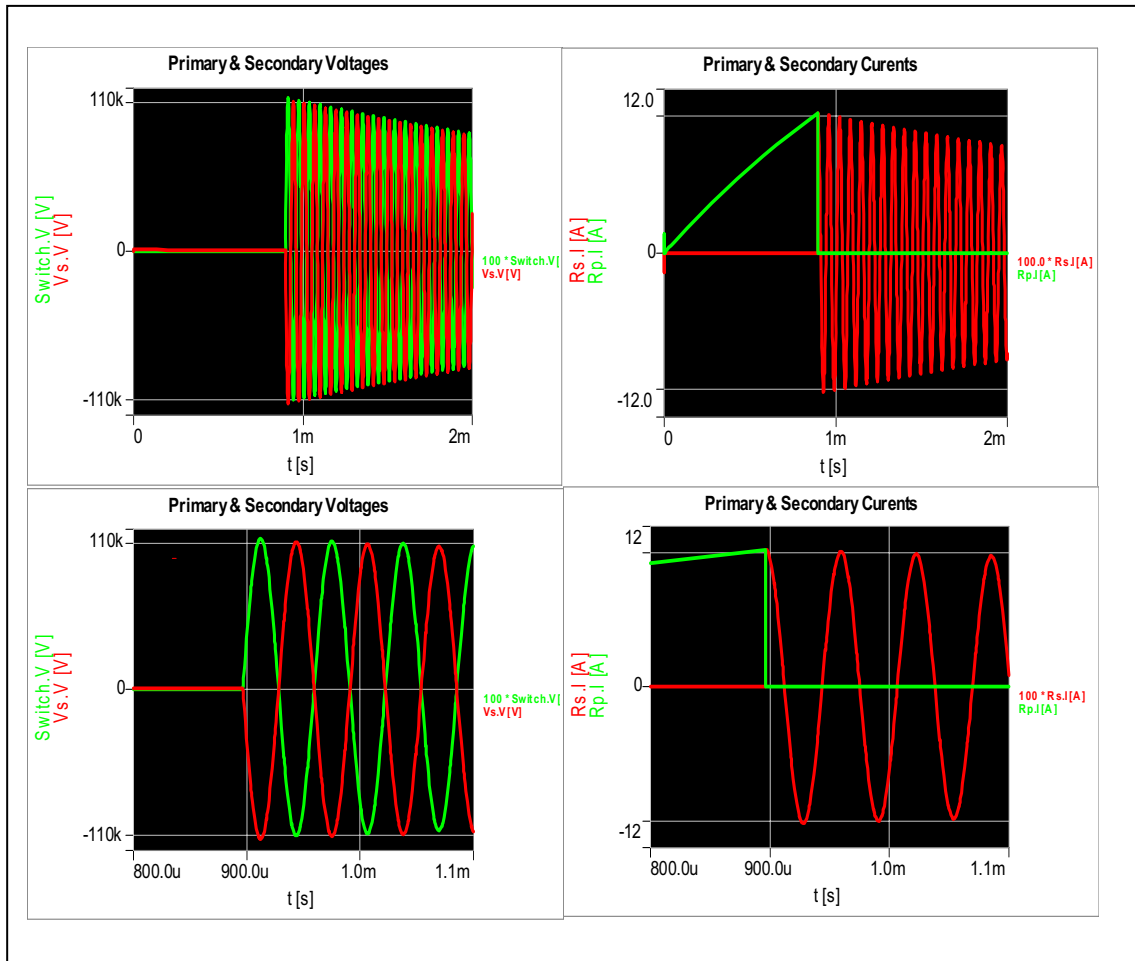


Fig. 5a. KV test:  $k = 1.0$ , no clamping diode, no  $C_{ps}$ . The traces are scaled:  $I_{primary} (\times 1)$ ,  $I_{secondary} (\times 100)$ ,  $V_{primary} (\times 100)$ , and  $V_{secondary} (\times 1)$ .

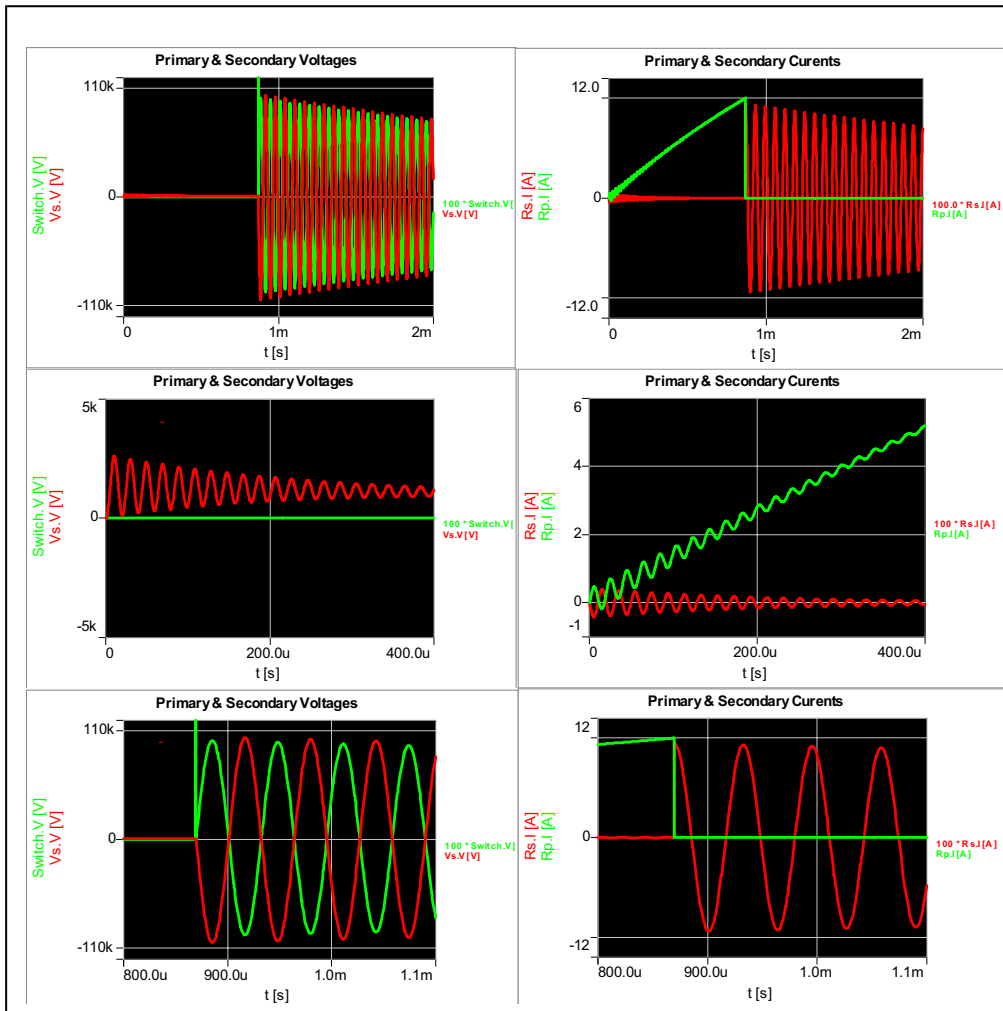


Fig. 5b. kV test:  $k = 0.95$ , no clamping diode, no  $C_p$

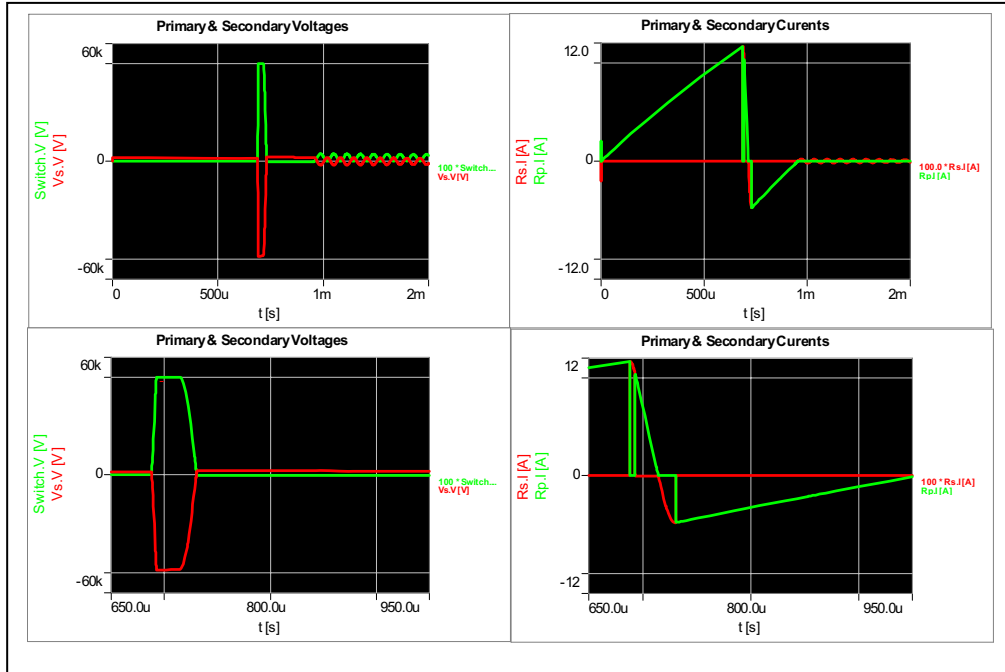


Fig. 5c. kV test:  $k = 1.0$ , with clamping diode, no  $C_{ps}$ .

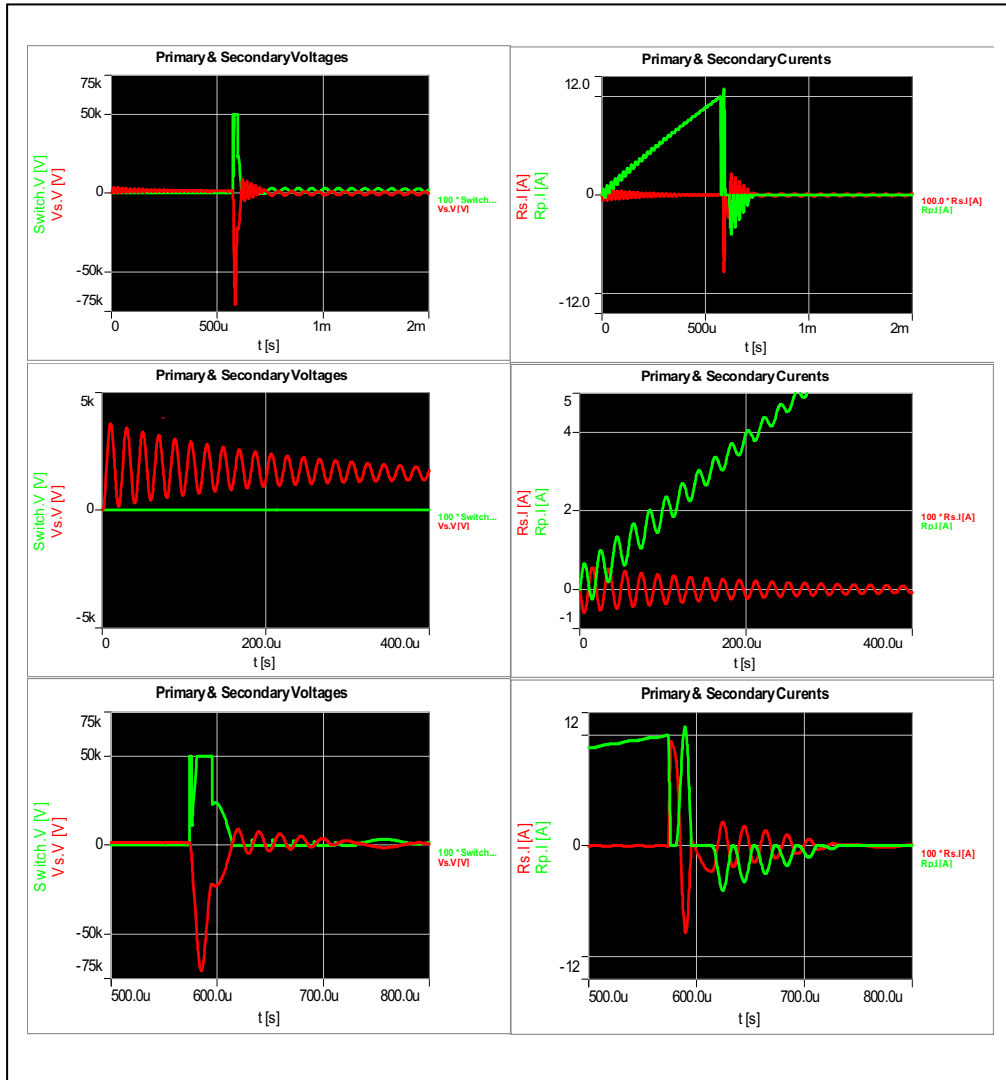


Fig. 5d.  $kV$  test:  $k = 0.95$ , with clamping diode, no  $C_{ps}$ .

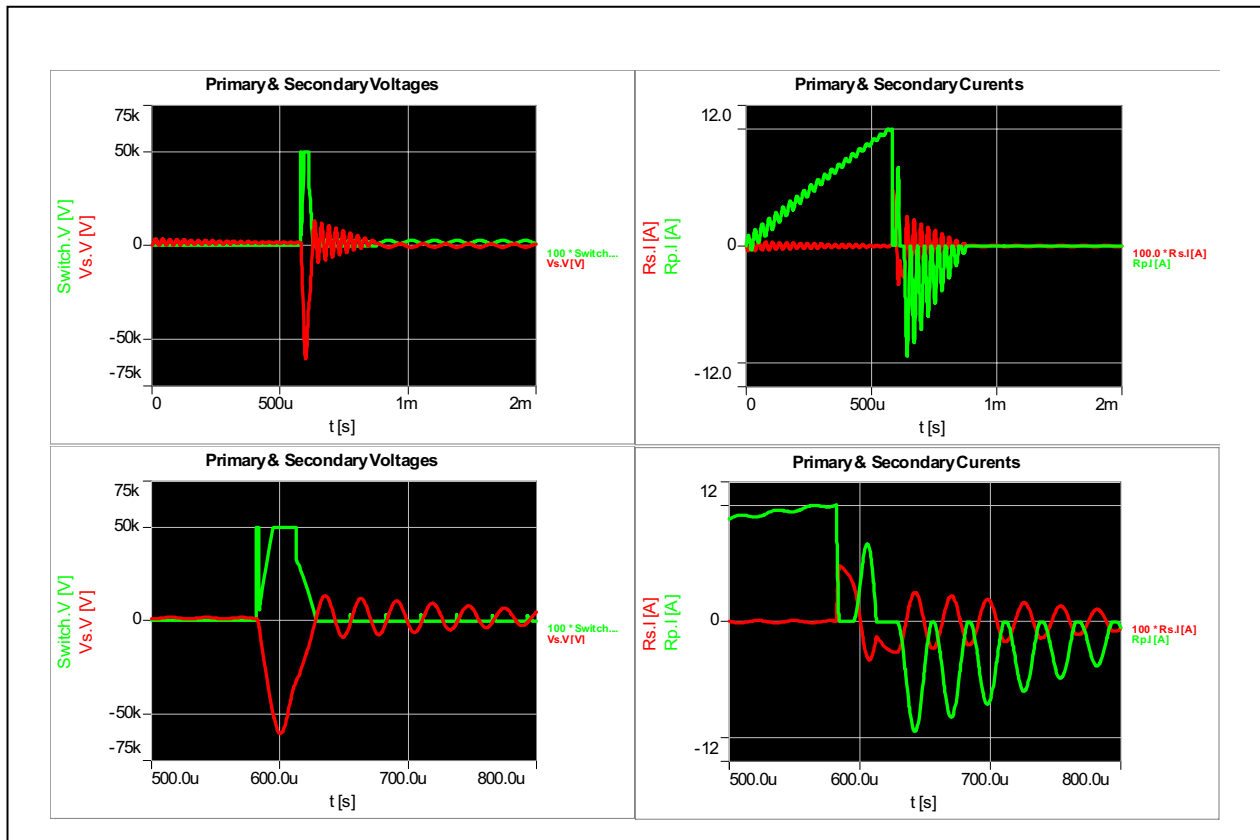


Fig. 5e. Case 1e.  $kV$  test:  $k = 0.95$ , with clamping diode, with  $C_p$

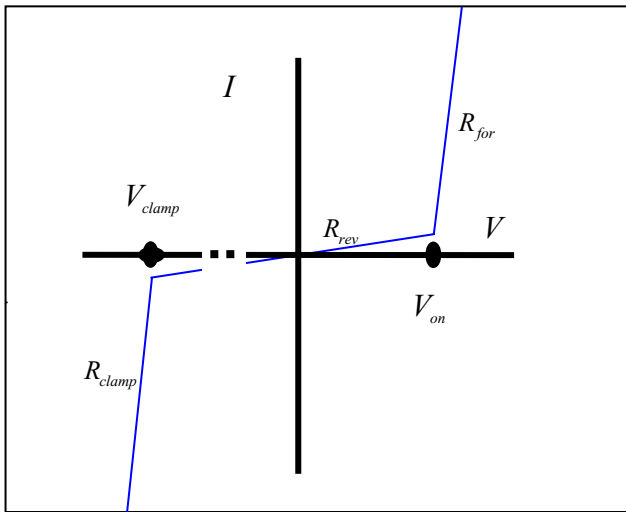


Fig. 6. Piecewise linear model for  $I$ - $V$  characteristics of Zener diode.

These last set of examples have indicated the origin of some of the salient features of the characteristic transient signals that can be observed from either data traces or simulated traces of real ignition coils. The simple coil model, with all features turned on, leads to surprisingly complex behavior of the coil system. For the  $kV$  test load, the addition of the clamping diode

certainly exhibits the most dramatic change in behavior over that of the fundamental circuit. Many of the features produced by the Simple Coil Model will be apparent in the actual data of an ignition coil, as well as the simulations of the Comprehensive Systems Model.

#### COMPREHENSIVE SYSTEMS MODEL

The Simple Coil Model discussed above provides guidance as to what behavior to expect from the transient signals of an ignition coil. Some other features are encountered in data traces from actual coils whose origins are less apparent to the uninitiated observer. Nevertheless, for the Simple Coil Model, one has to know before hand the values of the components to enter into the model. Accurate estimates of these values may be hard to determine, given the complicated geometry of actual coils.

The prototype coil that is discussed throughout the rest of this paper is illustrated in Figs. 8a and 8b. Observe that the secondary is not just a single coil, but is partitioned into bays. A bay is designed to limit the voltage difference between any two turns in that bay to a value below the dielectric breakdown determined by the wire coating and epoxy filling within the coil.

The bay structure leads to (electromagnetic) modeling complexity. This complexity is illustrated in Fig. 9. There are  $N+1$  (nonlinear magnetic) windings in the coil, if there are  $N$  bays. (for the prototype coil considered here,  $N = 8$ .) Each winding, interacts magnetically and electrically with all others. Hence, the  $2 \times 2$  Fundamental Coil Circuit inductance matrix,

$$\mathbf{L}_{fundamental} = \begin{bmatrix} L_p & M \\ M & L_s \end{bmatrix}$$

evolves to an  $(N + 1) \times (N + 1)$  inductance matrix for the Comprehensive Systems Model.

Similarly, instead of a the single capacitor,  $C_{ps}$ , coupling the primary and the secondary, as there is for the Simple Coil Circuit, there is a capacitance between the windings of each bay, and capacitance from each winding to the laminations.

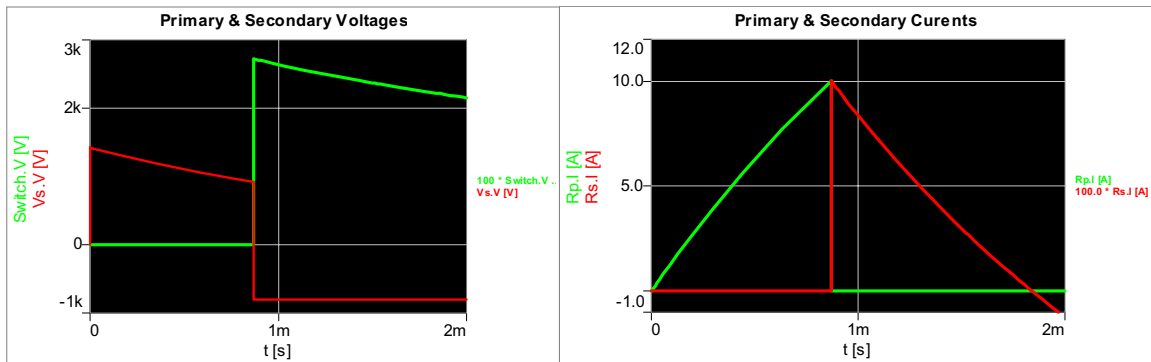


Fig.7a. Case IIa.  $E$  test:  $k = 1.0$ , no clamping diode, no  $C_{ps}$ .

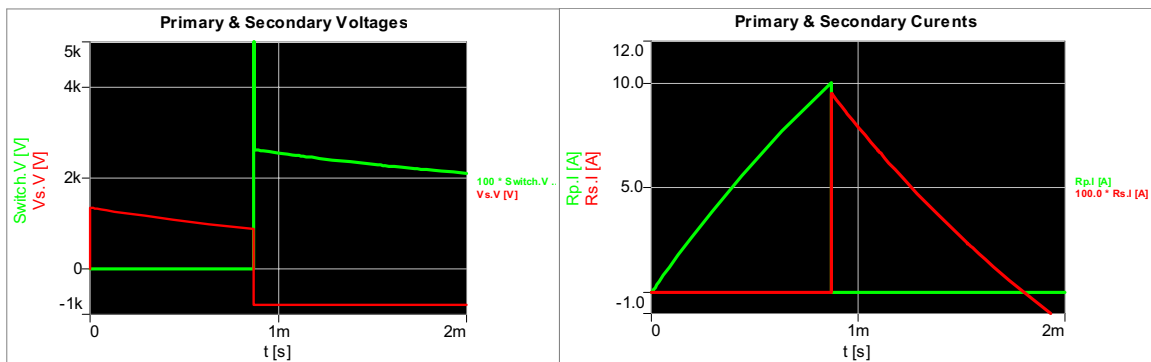


Fig.7b. Case IIb.  $E$  test:  $k = 0.95$ , no clamping diode, no  $C_{ps}$ .

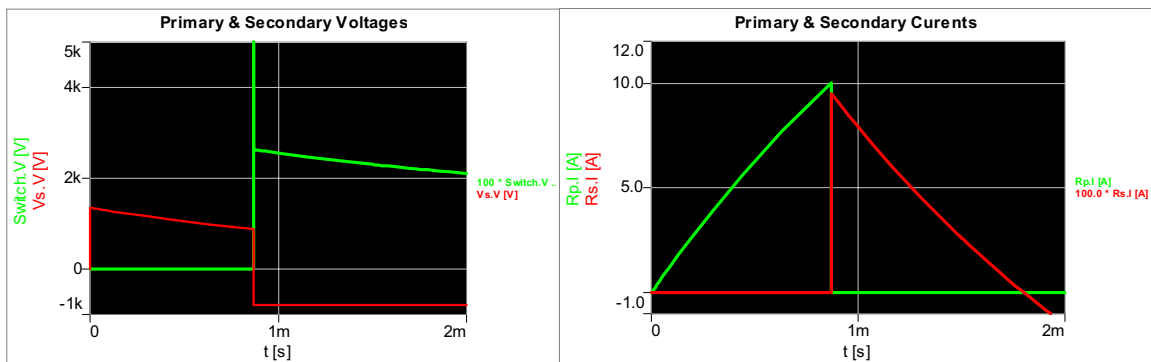


Fig. 7c. Case IIc.  $E$  test:  $k = 0.95$ , with clamping diode, no  $C_{ps}$ .

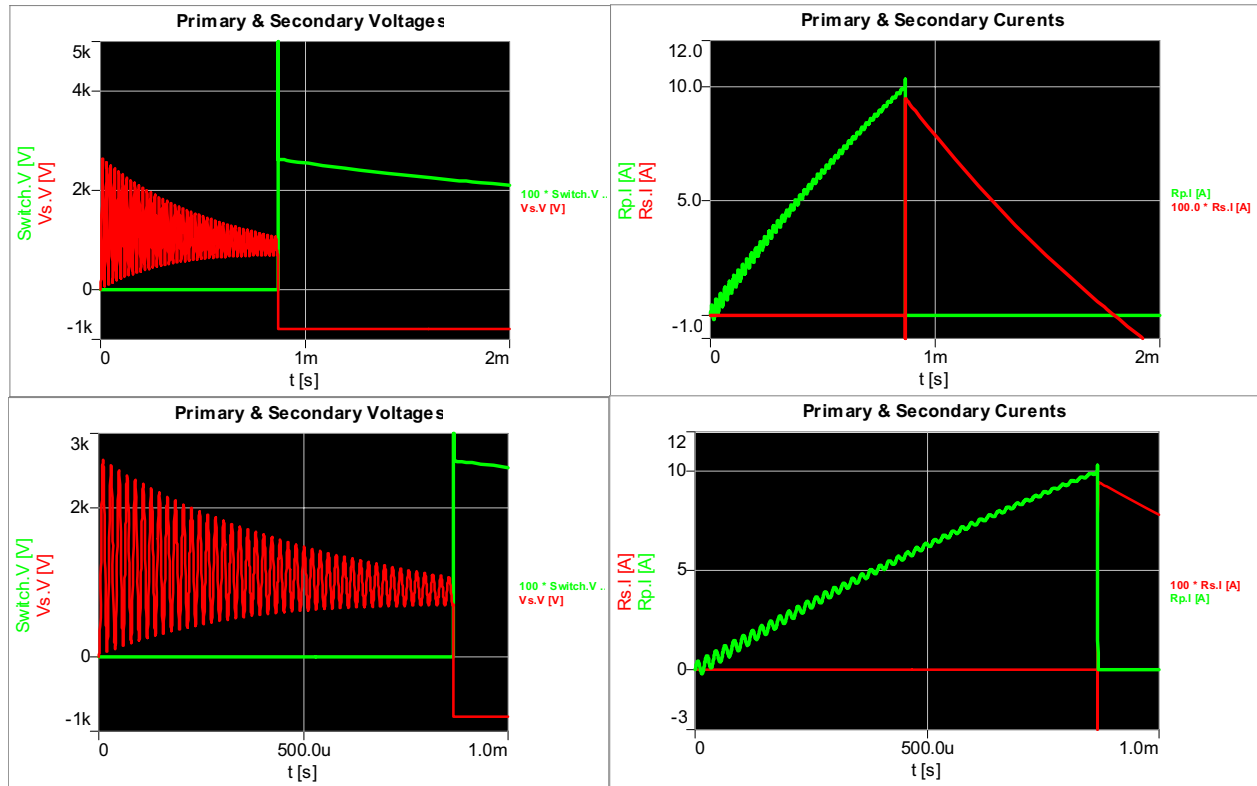


Fig. 7d. Case II d.  $E$  test:  $k = 0.95$ , with clamping diode, with  $C_{ps}$ .

In additions to the winding-to-winding capacitance, Fig. 9 shows a capacitance placed across the ports of each bay winding. These capacitors represent the turn-to-turn electrostatic interaction within a bay winding.

These capacitances exist, ultimately through dynamic effects, i.e., they result from the displacement current. For example, the secondary winding bay-to-bay capacitances would not exist from a purely DC electrostatic viewpoint, since the bays are part of the same long thin wire, i.e., all the bays are shorted together. From an electro-dynamic point of view, the bays do develop voltages with respect to one another. However, the approximation made to calculate the resulting dynamically induced capacitance is to use a DC electrostatic calculation that assumes the bays are disconnected from one another. The bays are reconnected later as part of a large circuit, such as that shown in Fig. 9. Similar statements hold for the turn-to-turn capacitance within a bay winding.

#### FEA calculations for Inductance and Capacitance

##### Winding-to-Winding Capacitance

In the case of the prototype coil under discussion, the geometry of the windings, in conjunction with the laminations, is inherently a 3D geometry; a 3D electrostatic FEA model for the capacitance calculation is appropriate.

In the formalism of the electrostatics for  $N_{con}$  conductors, in some specified volume  $\Omega$ , with a reference voltage  $V_0$ , where  $V_0$  is usually defined to be zero at “infinity”, the capacitance matrix  $[C_{ij}]$  connecting the charge,  $Q_i$ , on conductor  $i$ , with the voltage  $V_j$ , on conductor  $j$ , is defined by

$$Q_i = \sum_{j=1}^{N_{con}} C_{ij} V_j.$$

The matrix  $[C_{ij}]$  is symmetric, so that there are only  $\frac{1}{2} N_{con} (N_{con} - 1)$  independent elements.

Ansoft's electromagnetic FEA program Maxwell was used to determine the capacitance matrix for the complicated 3D geometry. Ansoft uses a different definition for the capacitance matrix:

$$Q_i = \sum_{j=0}^{N_{con}} \bar{C}_{ij} (V_i - V_j).$$

These capacitance elements are illustrated in Fig. 10. The relationship between the different formulations is,

$$C_{ij} = \begin{cases} -\bar{C}_{ij}, & i \neq j \\ \sum_{\substack{k=1 \\ k \neq i}}^{N_{con}} \bar{C}_{ik}, & i, j = 1, \dots, N_{con} \end{cases}$$

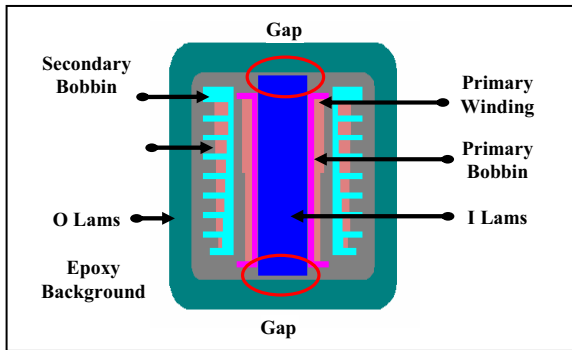
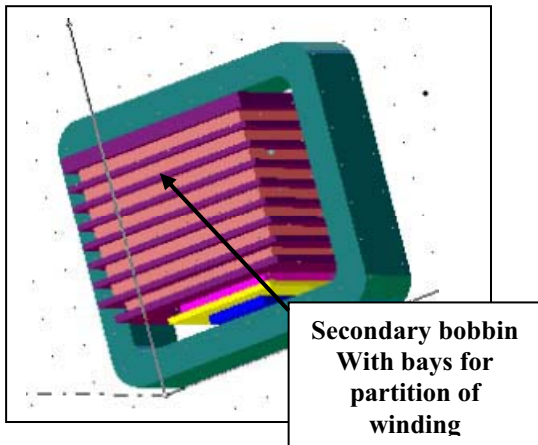


Fig. 8. (a) 3D Geometry of coil described in the text. The figure shows how the secondary winding is partitioned into several bays. The lamination structure consists of an O-lamination made of common grade steel, with the primary and secondary wound about a central I-Lamination made of orientated grade steel. (b) A 2D cross section of the coil in (a).

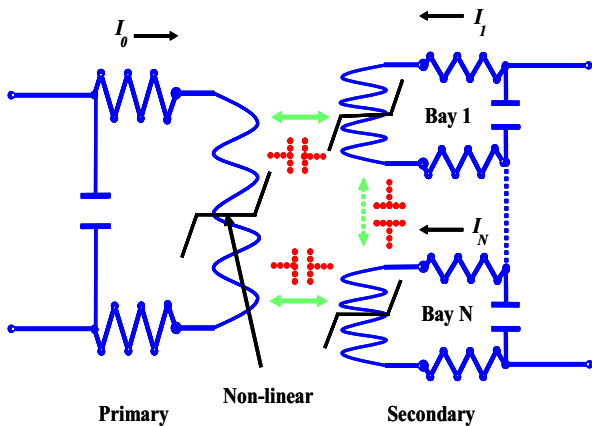


Fig. 9. Equivalent circuit model illustrating the complicated electromagnetic interactions among the parts of the primary and secondary windings.

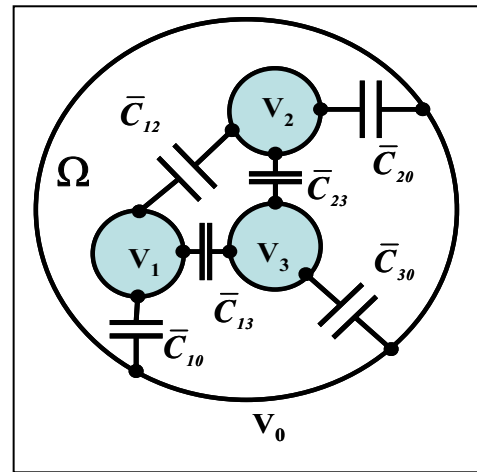


Fig. 10. Definition of capacitance matrix elements as used by the *Maxwell* FEA electromagnetic software. The volume  $\Omega$ , contains a set of perfect conductors, which will be at some constant voltage, either imposed or induced. The boundary of the volume is held at potential  $V_0$ , typically ground. Each conductor has a capacitance with respect to every other conductor, and to ground.

These capacitive interactions are included in the systems model through a multi-port lumped element formalism. FEA calculates the capacitance of the conductor array using the stored electrostatic energy  $\mathcal{E}^E$  (defined below) for the entire volume  $\Omega$  of the electrostatic field.

The physical system is assumed to be linear, therefore the response is proportional to excitation. For the electrostatic field, the excitation is the electric field  $\mathbf{E}$ , and the response is the displacement field  $\mathbf{D}$ . The linear relationship is

$$\mathbf{D} = \epsilon \mathbf{E}.$$

To be an electrostatic linear material, the dielectric constant  $\epsilon$  must not depend on the field  $\mathbf{E}$ . With the high potentials encountered in ignition coils, the linear material assumption breaks down to some extent. This non-linear behavior is beyond the scope of effort of modeling for this work.

The procedure for the capacitance calculation is outlined as follows. The first step in calculating the electrostatic energy is to assign a voltage  $V_j$  to conductor  $j$ , which produces an electric field throughout the volume  $\Omega$ . All other conductors, besides conductor  $j$ , are then grounded. The FEA program calculates both the electric field  $\mathbf{E}_j$ , and the displacement field  $\mathbf{D}_j$ , for the source on conductor  $j$ . This calculation is repeated for all (perfect) conductors in succession. Only  $N_{con}$  of these FEA field calculations are needed to obtain all  $N_{con}^2$

elements of the capacitance matrix. This is so because the capacitance between conductor  $i$  and conductor  $j$ , in terms of stored electrostatic energy, is

$$\mathcal{E}_{ij}^E = \frac{1}{2} \int_{\Omega} d\Omega \mathbf{E}_i \cdot \mathbf{D}_j \equiv \frac{1}{2} C_{ij} V_i V_j.$$

In the end, because of the linearity of the material, the electrostatic capacitance is purely a geometrical quantity; the value of the applied voltage is formally irrelevant.  $\mathbf{E}_i$  and  $\mathbf{D}_j$  are proportional to  $V_i$  and  $V_j$ , respectively, so that the magnitude of the voltages cancels in the calculation for the capacitance.

Typical value of the capacitance coupling the primary winding and individual bays is somewhere between  $\frac{1}{2}$  pF and 1 pF. The total primary-to-secondary capacitance might add to about 6 pF, hence 10 pF was chosen for  $C_{ps}$  for the Simple Coil Model.

Once the capacitance matrix has been calculated, the matrix can be exported as a circuit element to be used in simulation software. The equivalent circuit for the capacitive matrix appears in the *Simplorer* program as a graphical element, a block box, with a port corresponding to each conductor, i.e., winding or lamination.

## Coil inductance

### Magnetic material properties

Unlike the calculation of the capacitance matrix, the calculation of the inductance matrix for the coil is not a linear problem, although it is still a static problem. In the case of magnetic materials, the excitation-response relationship is in terms of the magnetic field  $\mathbf{H}$ , which is the applied field, and the magnetic induction  $\mathbf{B}$ , which is the response quantity. The  $\mathbf{B}$  field includes the magnetization  $\mathbf{M}$  of the material. The static relationship between  $\mathbf{H}$  and  $\mathbf{B}$  is a multi-valued curve, a hysteretic relationship, due to loss and meta-stability in magnetic domain motion [6]. Fig. 11 shows a series of static hysteresis curves, of ever increasing maximum field strength, for a nominal grade of laminated steel.

The multi-valued relationship is difficult to handle because it demands that the programmer keep track of history. Indeed, the situation is actually worse. In a dynamic, transient situation, such as occurs for the fluctuating signals of ignition coils, the actual path of the system in the H-B plane could be quite complicated. It will not follow the hysteresis curve, or any of the minor loops in entirety. The Jiles-Atherton formalism [7] might allow an adequate description for the dynamic case, but no commercial FEA software possesses such computational power at this time. The present commercially available software, including *Ansoft's Maxwell*, uses the standard engineering compromise for the multi-valued problem, the B-H curve.

For soft magnetic materials the B-H curve can be written as

$$\mathbf{B} = \mu(\mathbf{H}) \mathbf{H} \xrightarrow{\text{scalar}} B = \mu(H) H.$$

The magnetic permeability  $\mu$  is not a constant, but depends on the magnetic field. This constitutive relationship is a single-valued relationship, and approximately true for soft magnetic materials, because it represents an average behavior. If the hysteresis data is known, such as that of Fig. 11, the correct way to construct the B-H curve is to connect the tips of the minor hysteresis curves. In most cases, the data from the material supplier includes only the outer (largest) hysteresis curve. It is difficult to find the B-H curve from the outer hysteresis relationship. For lack of an alternative, an approximate B-H curve can be constructed by averaging the top and bottom branches of the hysteresis curve. Fig 12 shows the two B-H curves that were used in the analysis presented here. One curve is for nominal grade laminated steel, and the other is for better grade, oriented steel.

### Inductance from stored energy

In analogy with the determination of capacitance from stored electric field energy, the inductance of a set of windings can be calculated with the static magnetic stored energy  $\mathcal{E}^M$ . First, assume that the magnetic material is linear, so that the permeability  $\mu$  is constant. Then excite, in turn, each winding  $j$ , with a current  $I_j$ . The other windings are left unexcited. The application of current  $I_j$  to winding  $j$ , sets up fields  $\mathbf{H}_j$  and  $\mathbf{B}_j$ . The inductance  $L_{ij}$  between winding  $i$ , with turns  $N_i$  and winding  $j$ , with turns  $N_j$  can be written as:

$$\mathcal{E}_{ij}^M = \frac{1}{2} \int_{\Omega} d\Omega \mathbf{H}_i \cdot \mathbf{B}_j \equiv \frac{1}{2} L_{ij} (N_i I_i) (N_j I_j).$$

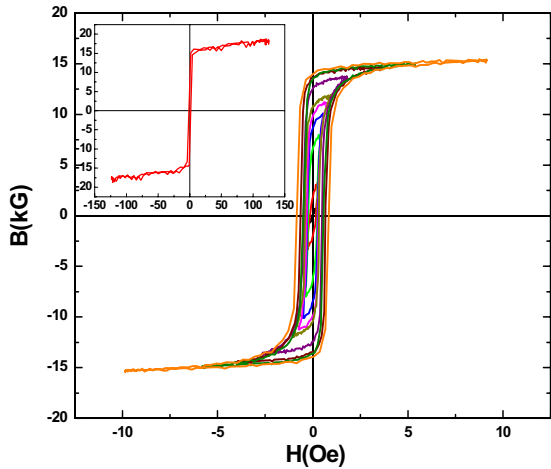
As shown in Fig. 9, if there are  $N + 1$  windings,  $N + 1$  FEA problems need to be run to obtain the  $(N + 1)^2$  matrix elements. Of course, the inductance matrix is also symmetric.

When the magnetic material is non-linear, the magnetic fields within the volume  $\Omega$ , and within the magnetic material in  $\Omega$ , will be a function of all the different currents. Consequently, so will the inductance. If there are  $N + 1$  windings, then there are  $N + 1$  different winding currents, so that

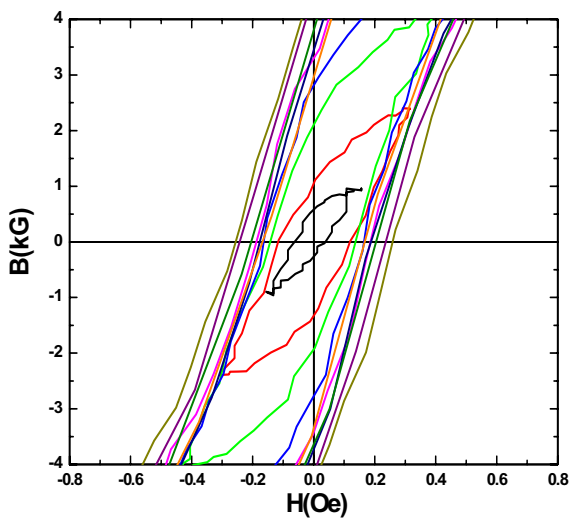
$$L_{ij} = L_{ij}(I_0, I_2, \dots, I_N), \quad i, j = 0, \dots, N.$$

There are two issues with respect to the calculation of non-linear inductance. The first issue is how to calculate inductance when that inductance depends on current. Secondly, there must be a way to deal with the fact that

the inductance depends on so many currents, nine in case presented in this paper. If there are  $N + 1$  windings, and each of the winding currents is sampled at  $S$  different values (to be used for interpolation), there are potentially a huge number of FEA case runs, namely,  $(N + 1)^S$ .



(a)



(b)

Fig. 11. (a) A series of hysteresis curves for ever increasing maximum field strengths. The insert show the outer hysteresis curve over a larger field range. (b) a close up view of the minor loops for low maximum fields. The data is in terms of traditional units used with magnetic materials (Oersteds for H, and Gauss for B) instead of SI units.  $1 \text{ Oe} = 1000/4\pi \text{ A/m}$ .  $1 \text{ G} = 10^{-4} \text{ T}$ .

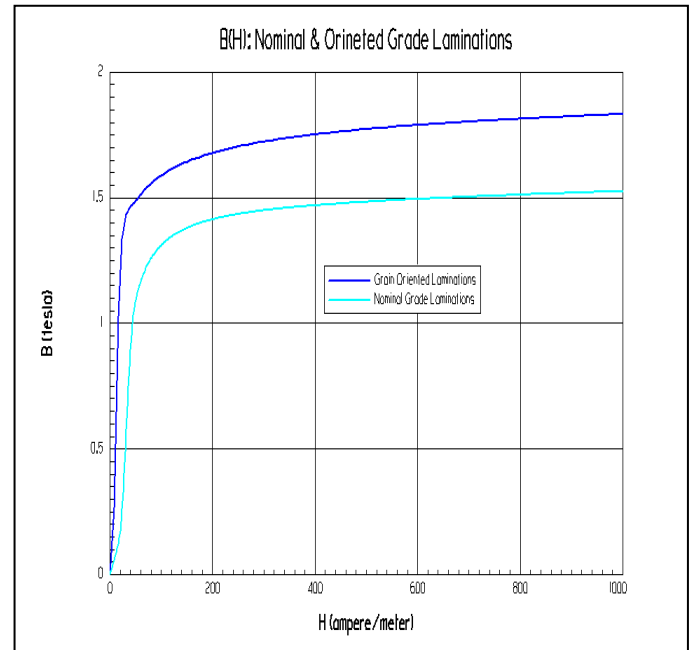


Fig. 12. BH curves for laminated steels used in this study. The bottom curve is for nominal grade laminated steel, the top curve is for a better grade (oriented) laminated steel.

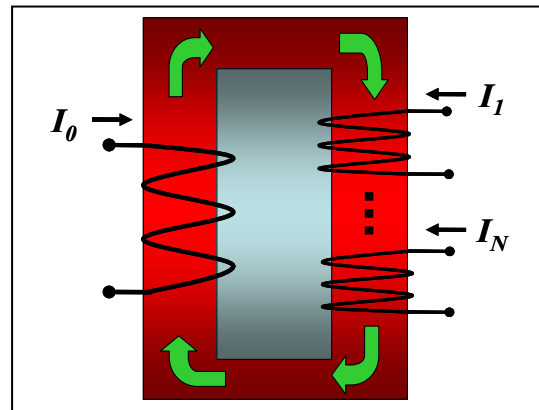


Fig. 13. Transformer Model: The model's basic assumption is that the total current,  $I_M$ , sets the state of the material, i.e., a permeability  $\mu(I_M)$ , by creating a magnetizing flux that links all the windings.

The method that *Ansoft* has chosen to deal with the first issue, the calculation of non-linear inductance, is to convert a non-linear problem to a locally inhomogeneous linear problem. A set of sample currents is specified by the user, and these currents are applied as sources in a set of magnetostatic FEA problems. For each sample current, the program computes an effective permeability for each point (finite element) in the material. Thus, a new effective material is produced for each current sample. The next step is to use the effective material as a base, and then perturb each current, in succession, by an incremental amount (in practice, say 1 A.) Then, the

inductance is calculated as in the case of a linear material:

$$\begin{aligned} \mathcal{E}_{ij}^M(I_0, \dots, I_N) &= \frac{1}{2} \int_{\Omega} d\Omega \mathbf{H}_i(\Delta I_i) \cdot \mu(I_1, \dots, I_N) \mathbf{H}_j(\Delta I_j) \\ &\equiv \frac{1}{2} L_{ij}(I_1, \dots, I_N) (N_i \Delta I_i) (N_j \Delta I_j), \\ i, j &= 0, \dots, N. \end{aligned}$$

This inductance calculation yields the so-called *apparent* inductance.

With regard to the second issue, i.e. the need to calculate the inductance for all combinations of current samples, the problem can be considerably simplified with a good engineering solution in the form the "Transformer Model". Fig. 13 shows the basic idea. It is assumed that the total current (magnetizing current)

$$I_M = \sum_{n=0}^N I_n$$

creates a magnetizing flux that essentially depends only on  $I_M$ , not the individual winding currents. This magnetizing flux then creates an effective permeability  $\mu(I_M)$ . One consequence of this approximation is that current needs to be applied only to one winding, typically the primary winding, and all other windings have zero current. The primary current is used to set the state of the material. Then, as before, the calculation of inductance returns to an inhomogeneous linear problem, and proceeds by applying incremental current to each winding in succession. With this scheme, the number of FEA case runs is reduced from  $(N+1)^S$  to  $S$ . With this approximation, some local variation, or saturation, in the material state is lost around secondary bay windings.

Similarly with the capacitance matrix, the FEA determined (non-linear) inductance can be exported as an equivalent circuit element to a simulation package. The exported inductance is a set of inductance matrices, one for each primary current sample. The inductance matrices were determined in a magnetostatic calculation, but dynamic effects can be accommodated through interpolation between inductance matrices generated by neighboring currents. The inductive circuit element appears as a graphical black box element with  $N+1$  pairs of ports in the simulation software.

### Single Bay Winding Capacitance

This single bay winding capacitance arises from the array of hundreds of coated copper wires, wound in essentially a hexagonal close-packing configuration, in each secondary bay. Each wire has a diameter of approximately 50  $\mu\text{m}$ . The winding density is about 300 turns/mm<sup>2</sup>.

A series of modeling approximations are made to make the problem of determining the capacitance reasonably manageable, as a first attempt at this problem. Fig. 14a shows a schematic of a bay winding. The bay winding is inherently a 3D structure, but to simplify this structure, the helical winding is approximated by a series of disconnected stacked rings. Secondly, the structure is converted to a 2D axisymmetrical geometry. In the xy-plane, the bays have a rectangular cross section. To create a 2D axisymmetric problem, the rectangular base of the winding is converted to a circular geometry with an effective radius. The effective radius is determined so that circular perimeter equals the rectangular perimeter as illustrated in Fig. 15. Fig. 16 show the resulting geometry used for an axisymmetric 2D electrostatic calculation.

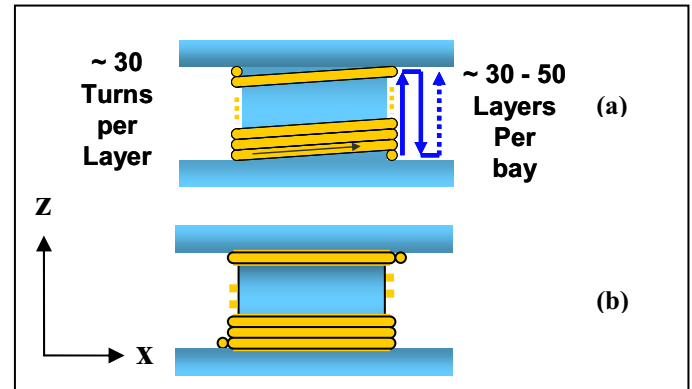


Fig. 14. (a) A schematic of the winding for a single secondary bay. The winding is helical for each layer, but successive layers oscillate in winding direction. (b) the approximation of this winding structure in terms of a series of stacked rings.

Although the geometry is simplified, the problem is still large since the bays can still be filled with up to a thousand turns of wire. FEA can be used to perform the electric field calculations, given the geometry and parameters of the materials, such as the wire coating, epoxy fill, and bobbin plastic. The wire cores are assumed to be perfect conductors, so that no field is determined within a wire core. FEA is used to solve for the capacitance matrix for the interactions between all wire cores. Once this matrix is obtained, the general relationship between stored electrostatic energy and capacitance is used to determine the capacitance for the bay winding, given the winding scheme of a bay.

To this end, the electrostatic energy for a configuration of  $N_{turns}$  conductors, each excited with an applied potential, is given as

$$\mathcal{E}^E = \frac{1}{2} \int_{\Omega} d\Omega \mathbf{E} \cdot \mathbf{D} = \frac{1}{2} \sum_{m=1}^{N_{turns}} \sum_{n=1}^{N_{turns}} C_{mn}^{Bay} V_m V_n.$$

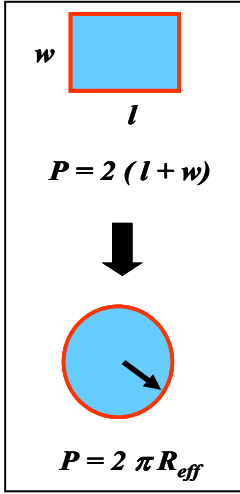


Fig. 15. We change the 3D geometry of a winding to an approximate 2D axisymmetrical geometry by creating an effective circular cross section from the rectangular cross section of the bays.

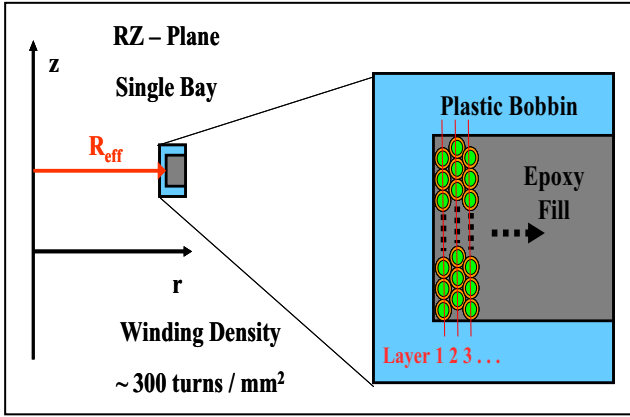


Fig. 16. The axisymmetric geometry used to calculate the turn-to-turn capacitance matrix for the winding configuration of a secondary bay.

The number of conductors in a bay is assumed to be equal to the number of wire cores in a bay, which is equal to the number of turns  $N_{turns}$ . In this configuration, core  $m$  has an applied potential voltage,  $V_m$ . The matrix  $[C_{mn}^{Bay}]$  is that calculated by the electrostatic FEA. The winding scheme is introduced by labeling the winding cores in the order that they appear in the winding. An additional modeling assumption is that the voltage increases linearly with the core label, and that there is a voltage,  $\Delta V$  between successive turns. Thus,

$$V_m = m \Delta V.$$

The stored energy is then

$$\mathcal{E}^E = \frac{1}{2} (\Delta V)^2 \sum_{m=1}^{N_{turns}} \sum_{n=1}^{N_{turns}} m n C_{mn}^{Bay}.$$

The effective capacitance  $C_{eff}^{Bay}$  of the configuration can be defined through the relation

$$\mathcal{E}^E = \frac{1}{2} C_{eff}^{Bay} V_{eff}^2,$$

where  $V_{eff}$  is the effective voltage across the top and bottom turns (the first and last rings of the winding); here

$$V_{eff} = (N_{turns} - 1) \Delta V.$$

Thus, the effective capacitance of the bay, in terms of all of the turn-to-turn capacitances is

$$C_{eff}^{Bay} = \frac{1}{2 (N_{turns} - 1)^2} \sum_{m=1}^{N_{turns}} \sum_{n=1}^{N_{turns}} m n C_{mn}^{Bay}.$$

There is a catch in the calculation of the capacitance matrix  $[C_{mn}^{Bay}]$ . The computer quickly runs out of memory when the number of wire cores approaches several hundred. Therefore, there is a need for a method to extrapolate the value of the effective capacitance for a large number of turns from a smaller number of turns.

As a function of the number of winding layers  $N_{layers}$ , the effective capacitance can be postulated to have the following form:

$$C_{eff}^{Bay} (N_{layers}) = C_0 + \frac{C_1}{N_{layers}} + \frac{C_2}{N_{layers}^2}.$$

The form of this fitting function is suggested by the fact that the capacitance depends on the inverse square of  $N_{turns}$ , and the number of layers increases proportionally with the number of turns.

Regardless of original justification for the functional form, it can be checked for self consistency as follows: The bay capacitance is calculated using the procedure and formulas described above, for, say, a middle bay in the secondary winding, and for a low number of layers, such as  $N_{layers} = 2, 4, \text{ and } 8$ . Then,  $C_0$ ,  $C_1$ , and  $C_2$  can be determined. The determination of these constants fixes the curve. Fig. 17 shows such a curve, where the capacitance values are normalized. To validate the fitting function, the capacitance for  $N_{layers} = 1, \text{ and } 16$  are calculated as a self consistency check. The figure shows that these data points fall on the fitting curve.

## COMPARISON OF TEST DATA AND SIMULATION

### SYSTEMS MODEL

With the computational machinery that has been assembled, the time transient traces and the frequency domain traces for the prototype coil were generated. To create these simulations, a Comprehensive Systems Model was constructed with the graphical user interface of *Ansoft's Simplorer* simulation software. Fig. 18 shows a graphical representation of the systems model. The systems model includes modules for the coil driver, the coil, and the coil loads.

For the coil model, there is an inductance equivalent circuit and a winding-to-winding capacitance equivalent circuit, which is implemented as two half models. These circuits are black boxes presented to the user as devices with appropriate ports. As described above, a capacitor across each secondary bay is also included to account for the turn-to-turn capacitance of each bay. Series resistors are included to account for the winding resistance, which is simply calculated for the length, diameter, and resistivity of the wire. In addition, an estimated value for a shunt resistor is included to account for a core loss. The detailed procedure to estimate this resistance is not described here, but it was generated with the use of *Ansoft's* transient magnetic solver, coupled with material loss data.

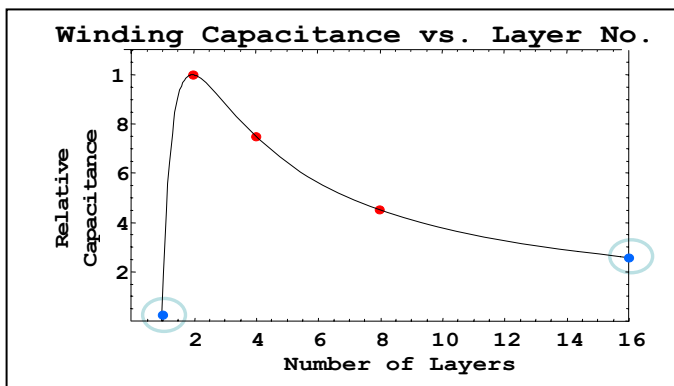


Fig. 17. Bay winding capacitance calculated by the fitting function,  $C_{eff}^{Bay}(N_{layers}) = C_0 + C_1 / N_{layers} + C_2 / N_{layers}^2$ . The middle three data points, for  $N_{layers} = 2, 4,$  and  $8$ , in the graph were used to fix the three fitting constants. The first and last data points were calculated as a self-consistent check. These last two points fell on the curve.

The driver portion of the systems model was constructed to include a battery, an idealized IGBT switch, and a 410 V Zener clamping diode. A second Zener diode, opposing the clamping diode, was needed to better match data; it represents something of the electrical circuit comprising the IGBT. The driver sub-model is the

weakest part of the systems model. It was difficult to obtain a working model from the IGBT supplier.

As for the ignition coil loads in the systems model, a 25 pF capacitive load is used for the  $kV$  test, and an 800 V Zener load for the  $E$  test.

### TRANSIENT SIMULATION

Figs. 19 and 20 display the results of the transient coil simulations, and compare the simulations and corresponding tested data traces. The simulation traces match the test data very well in most cases. The simulation falls short in the case of the  $kV$  experiment for the primary and secondary voltages. These signals are quite sensitive to the model for the IGBT and clamping diodes. Thus, the simulations point to further development of faithful IGBT models.

These simulations were generated from a first principles formulation. With regard to the coil parameters used in the simulation, there was no adjustment, except for some estimation of stacking factor. The parameters associated with the driver model required the most adjustment.

### FREQUENCY DOMAIN SIMULATION

The simulations in the time domain matched the test data well. However, different combinations of parameters could lead to the same result. One sensitive test of the model is to probe the resonant structure of the secondary. Fig. 21 shows an impedance sweep of magnitude and phase for the secondary winding. Fig. 21 shows a fit to this test data. The coil model used to generate the frequency domain simulation is the same as for the time domain. When comparing the test data and simulation in the frequency domain, it can be seen that the simulation approximately duplicated the resonance structure of the secondary. Although the positions of the higher order resonant frequencies did not precisely match with the test data, the number, relative position, and height of resonances, are reproduced fairly well by the simulation.

The frequency domain simulation indicates that the model of the internal electromagnetic structure of the coil has fidelity. The model reflects reality.

As a technical matter, for the frequency domain simulation, one could not use an inductance matrix generated for the normal range of currents encountered in the time domain. The frequency domain data is gathered at very low voltage and current. The B-H curve is not accurate at the low currents (or correspondingly low fields.) The inductance at very low fields appears to be much lower than that predicted by the B-H curve, derived from the material supplier. The B-H curve is not typically well characterized at low fields. To produce the lower inductance needed to match the simulation with

the data, an inductance matrix generated for very high MMF (2000 A-Turns). At this high MMF (of high field), the B-H curve goes into saturation, and the inductance is reduced over that of the unsaturated region of the B-H curve since the inductance is proportional to the slope of the BH curve. In this way we generated a lower inductance from our standard BH curve, but the resulting mutual inductances may not be quite correct, which could lead to incorrect predictions for high frequency modes.

## CONCLUSION

This paper has presented a comprehensive method for modeling automotive ignition coil systems. The proposed model simulates all aspects of the electromagnetic structure of the coil. The predictions of this comprehensive model were validated by test data in both the time and frequency domains. The agreement between test data and simulation demonstrates that the proposed modeling method has high fidelity, and thus will be a valuable tool to the coil design engineer.

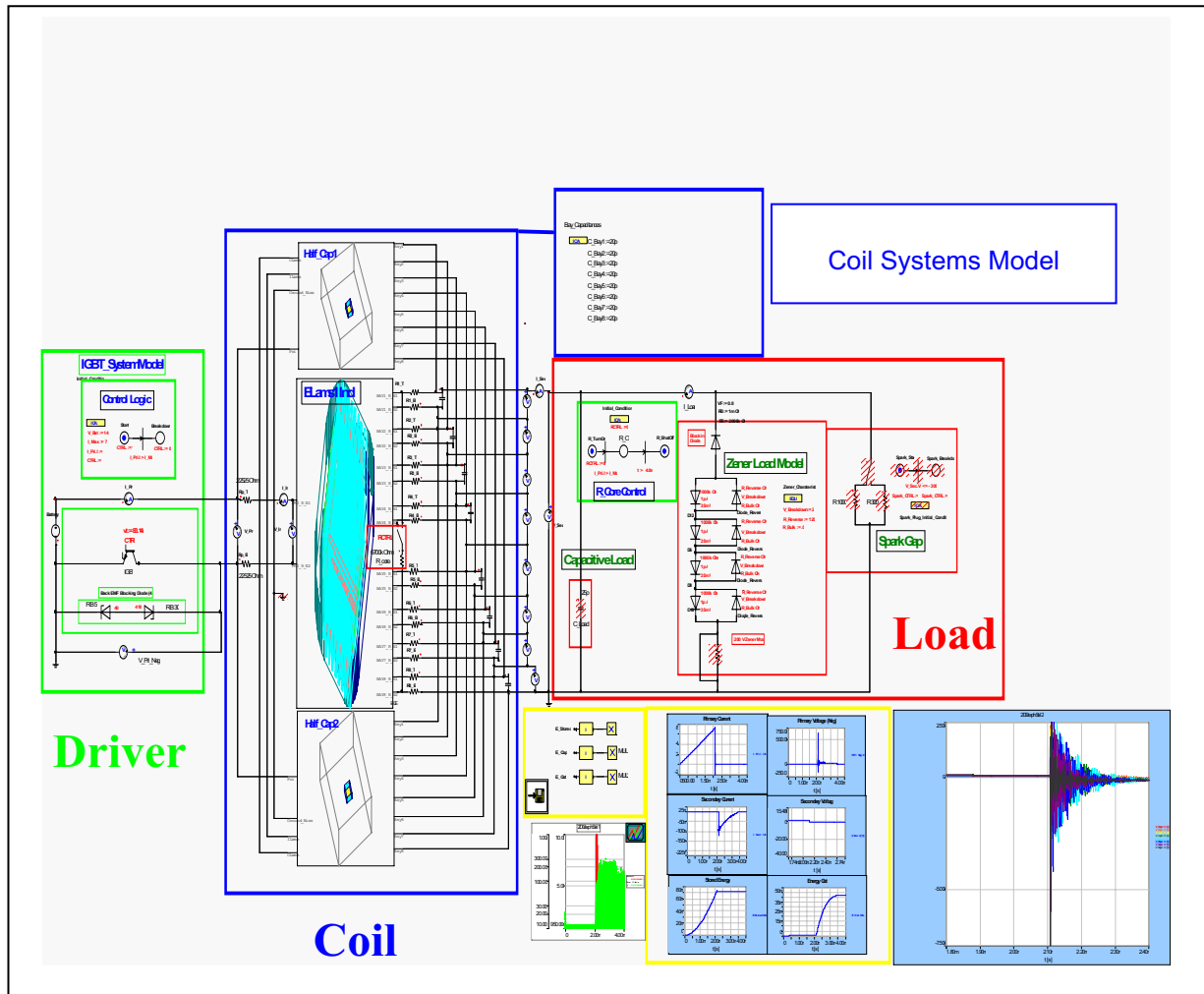


Fig. 18. A graphical representation of the systems model for the ignition coil. The systems model includes a sub-model for the driver, one for the coil, and one for the loads

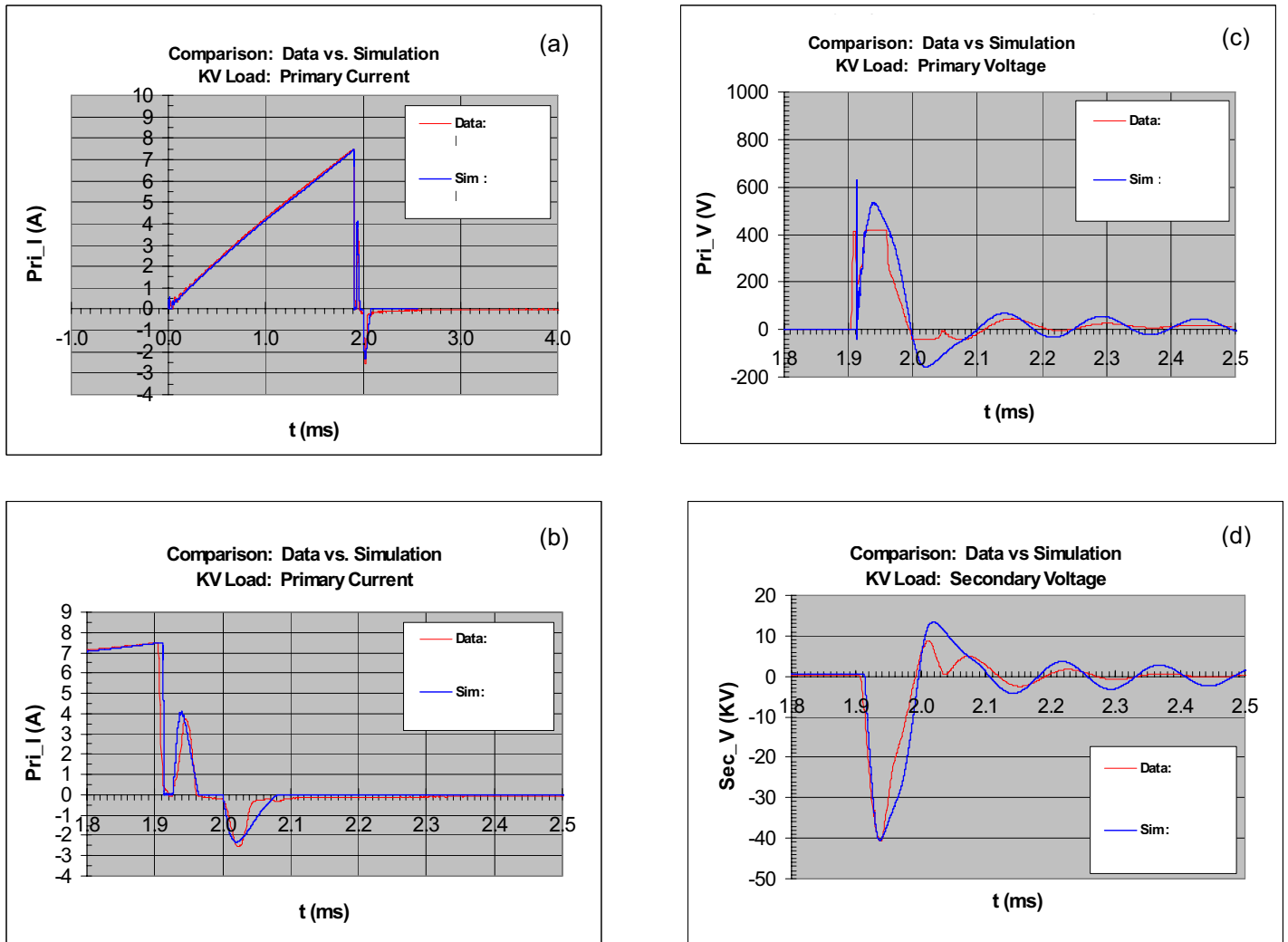


Fig. 19. Transient signals from the *kV* test for the coil under study. (a) Primary current charging curve, both a test data trace and the corresponding simulation. The test data and simulation exhibit the post breakdown current pulses due to the Zener diodes across the primary switch. (b) Magnified view of the primary current. (c) The primary “fly back” voltage. Note that the simulated signal does not display the proper flat top, as does the test data. The flat top in the test data is due to the Zener avalanche voltage. The reason that the simulated trace overshoots is due to the inadequate model for the IGBT. The resistances in the characteristics of the Zener can be adjusted so that the post breakdown pulses of the primary current had the correct magnitudes. Nevertheless, the increased resistances used in the simulation to match the peaks of the primary current pulses reduced the sharpness of the knee for the voltage avalanche of the Zener. (d) Secondary voltage traces for the test data and simulation. The secondary voltage simulation has the correct amplitude, but not quite the correct shape. Part of the reason for the incorrect shape is again due to the inadequate IGBT model.

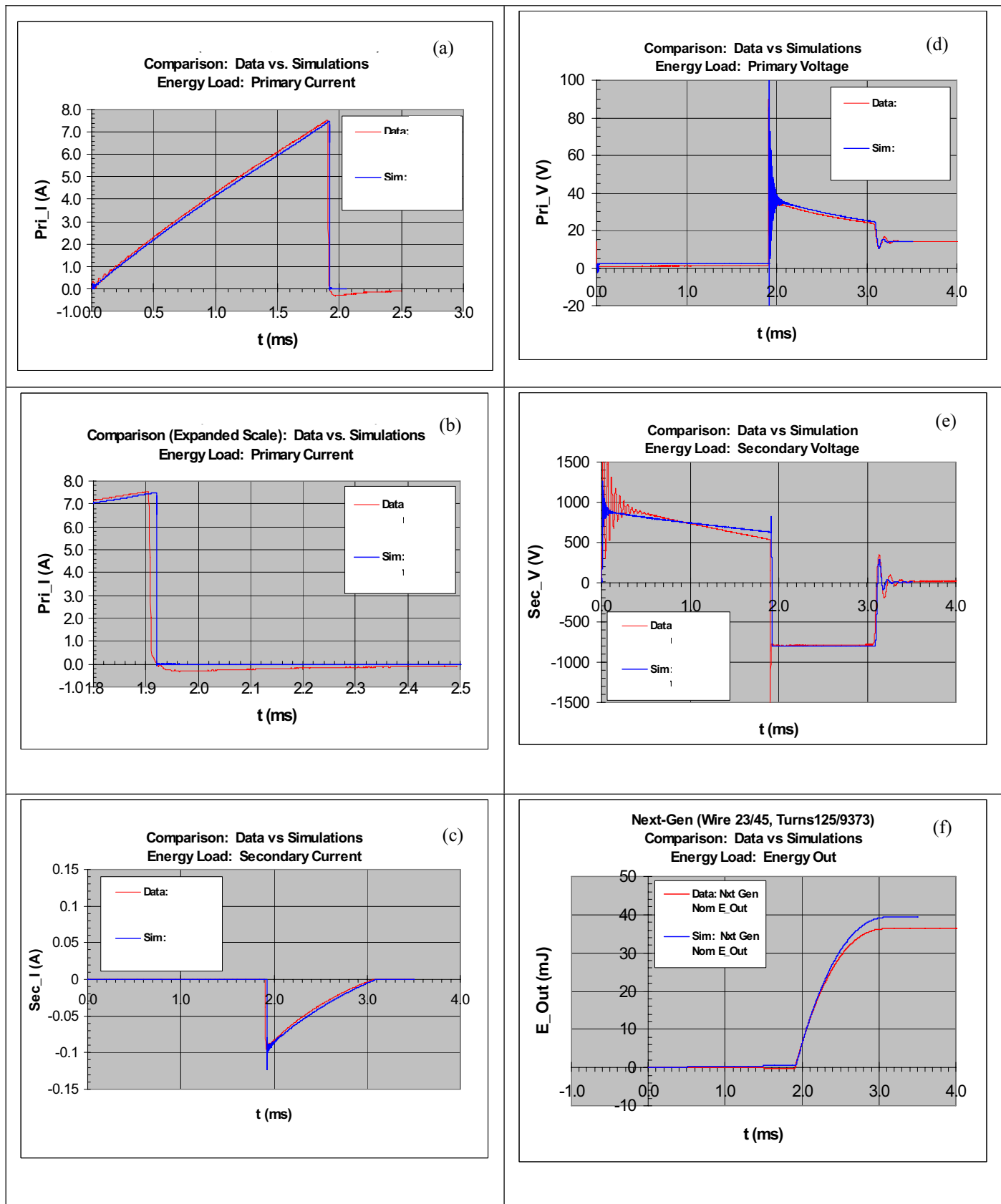


Fig. 20. Test data and simulation results of the  $E$  Test transient signals for the coil under study. (a) Primary current charging curve. (b) Magnified view of primary current. (c) Secondary current. (d) Primary “fly back” voltage trace, a reflection of the secondary voltage. (e) Secondary voltage traces. (f) Cumulated energy out of the secondary.

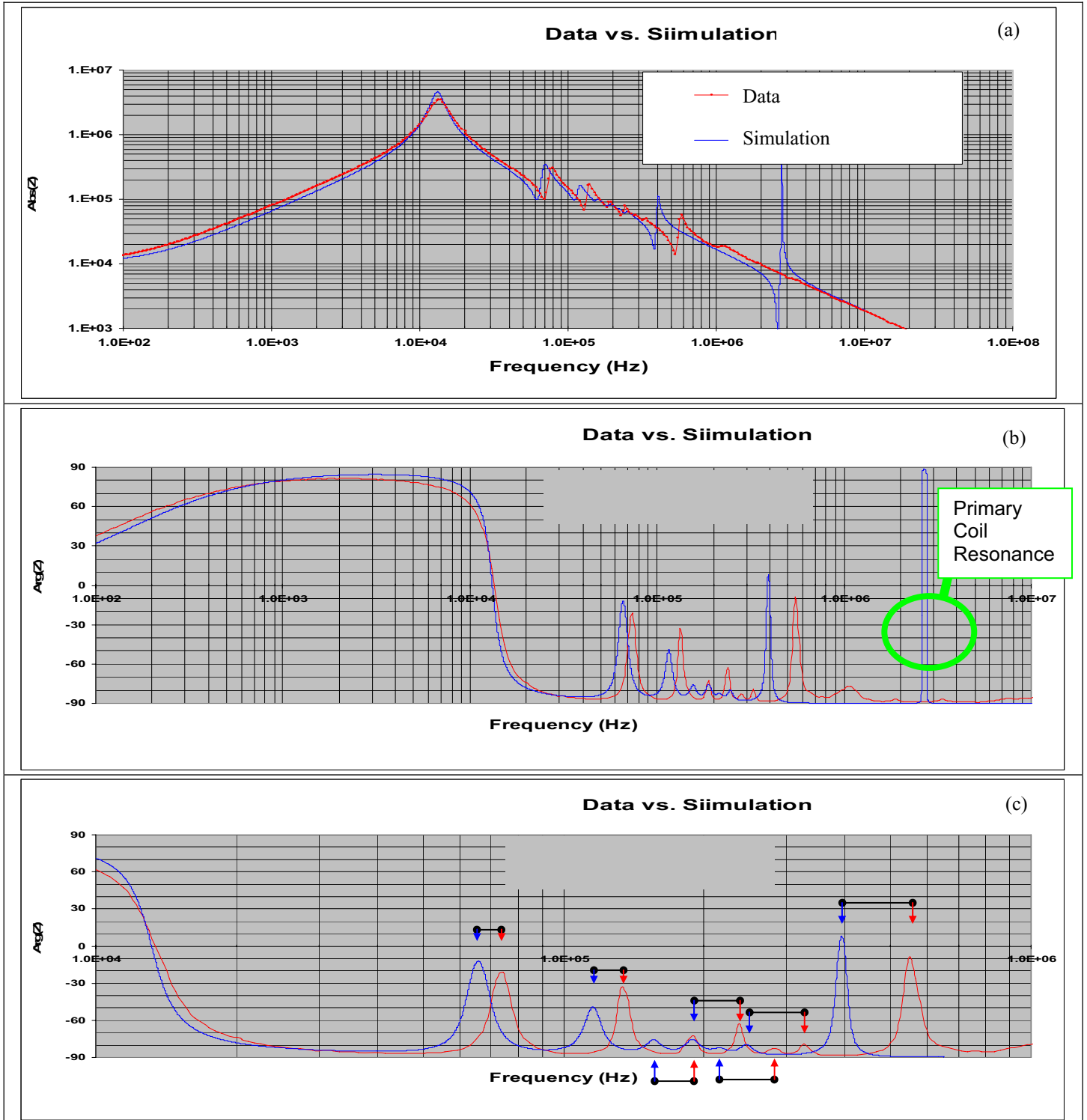


Fig. 21. Test data and simulation results for frequency domain impedance sweeps of secondary coil. (a) Impedance magnitude. (b) Impedance phase. (c) Magnified view of impedance phase. The pairs of arrows indicate the correspondence between resonances in the test data and simulation. There is a one-to-one correspondence in the resonances: the heights of the peaks tend to correlate, but imperfectly, and the position of corresponding resonances are correlated, but shifted.

## REFERENCES

[1] Donnelly, J. Michael, Gauen, Kim, "New IGBTs and simulation models simplify automotive ignition system design", IEEE Annual Power Electronics Specialists Conference, 1993, p 473-481.

[2] Rohwein, G.J., Babcock, S.R.; Buttram, M.T., Camilli, L.S., "Advanced automotive ignition systems", Digest of Technical Papers-IEEE International Pulsed Power Conference, v 1, 1995, p 40-45.

[3] Yedinak, J., Merges, J.; Wojslawowicz, J., Bhalla, A., Burke, D., Dolny, G., "Operation of an IGBT in a self-clamped inductive switching circuit (SCIS) for automotive ignition", IEEE International Symposium on Power Semiconductor Devices & ICs (ISPSD), 1998, p 399-402.

[4] *Simplorer*™ simulation system, Version 7.0, Ansoft Corporation, 225 West Station Square Drive, Pittsburg, PA, 15219-1119. For the simple coil models, we employed only the "Student Version", of *Simplorer*™, which can be obtained for free from a download at the Ansoft website, [www.ansoft.com](http://www.ansoft.com).

[5] *Simplorer*™ uses two opposing diodes, in parallel, as a model for a Zener diode. The characteristics of the diodes are static; the forward diode uses an exponential function, while the reverse diode uses a piecewise linear mode function for the diode characteristics.

[6] Bertotti, G., "Hysteresis in magnetism: for physicists, material scientists, and engineers." Academic Press, 1<sup>st</sup> ed., June 15, 1989.

[7] Petrovic, P., Mitrovic, N., Stevanovic, M., Pejovic, P., "Hysteresis model for magnetic materials using the Jiles-Atherton model", AUTOTESTCON (Proceedings), 1999, p 803-808.

## CONTACT

Dr. Chris Mi, Ph.D,  
Senior Member IEEE, Member SAE  
Assistant Professor  
Department of Electrical and Computer Engineering  
University of Michigan - Dearborn  
4901 Evergreen Road, Dearborn, MI 48128 USA  
Tel: (313)583-6434  
Email: [chrismi@umich.edu](mailto:chrismi@umich.edu)

## DEFINITIONS, ACRONYMS, ABBREVIATIONS

|            |   |             |  |
|------------|---|-------------|--|
| <b>B</b>   | Magnetic induction                                      |             |  |
| <b>D</b>   | Electric displacement field                             | $N_p$       | Number of turns in primary coil  |
| $\Phi_M$   | Magnetizing flux  | $N_s$       | Number of turns in secondary coil  |
| <b>H</b>   | Magnetic field  | $n$         | Turns ratio  |
| $I_{\max}$ | Maximum primary current                                 | $\tau_B$    | Time at which the controlled switch opens  |
| $i_p$      | Primary transient current                               | $\tau_p$    | Primary winding time constant  |
| $i_s$      | Secondary transient current                             | $\tau_s$    | Secondary winding time constant  |
| <b>J</b>   | Current density field                                   | $\tau_{SD}$ | The spark duration, or the time for which the secondary current is non-zero in an $E$ test |
| $L_p$      | Inductance of primary winding                           | $v_p$       | Primary transient voltage  |
| $L_s$      | Inductance of secondary winding                         | $v_s$       | Secondary transient voltage  |
| $M$        | Mutual inductance between primary and secondary winding |             |  |
| <b>M</b>   | Magnetization field of magnetic material                |             |  |